Optimizing the performance of a monolithic Tm 3+ , Ho 3+ -codoped fiber laser by FBG reflected wavelength and fiber gain matching

Arnaud Motard, Christophe Louot, Inka Manek-Hönninger, Nicolas Dalloz, Anne Hildenbrand-Dhollande

Research Article Vol. 31, No. 12 / 5 Jun 2023 / Optics Express 18939
Optics EXPRESS

Optimizing the performance of a monolithic Tm^{3+}, Ho^{3+}-codoped fiber laser by FBG reflected wavelength and fiber gain matching

ARNAUD MOTARD,[1,2,*] CHRISTOPHE LOUOT,[1] INKA MANEK-HÖNNINGER,[2] NICOLAS DALLOZ,[1] AND ANNE HILDENBRAND-DHOLLANDE[1]

[1] French-German Research Institute of Saint-Louis, 68300 Saint-Louis, France
[2] Université Bordeaux, CNRS, CEA, CELIA UMR5107, F-33405 Talence, France
[*] arnaud.motard@isl.eu

Abstract: We present the optimization of a 2.1-µm continuous wave monolithic single-oscillator laser by adapting the Fiber Bragg Grating (FBG) reflected wavelength to the maximum gain wavelength of the Tm^{3+}, Ho^{3+}-codoped fiber. Our study examines the power and spectral evolution of the all-fiber laser and demonstrates that matching these two parameters improves the overall performance of the source.

1. Introduction

The development of all-fiber single oscillator monolithic laser sources at 2 µm has been a significant challenge in recent years. These sources offer the compactness and robustness necessary for many 2-µm applications, such as surgery, LIDAR, and directed countermeasures [1–4]. 2-µm fiber lasers have traditionally used thulium-doped (Tm^{3+}) active media pumped at 793 nm to generate efficient laser emission at a wavelength of 1.95 µm [5,6]. To produce efficient radiation at around 2.1 µm, a holmium-doped (Ho^{3+}) fiber can be pumped at 1.95 µm using a thulium-doped fiber laser. In 2013, Hemming et al. reported the highest output power ever achieved from a Ho^{3+} doped fiber laser, generating a maximum output power of 407 W at 2.12 µm. The laser employed an array of six thulium-doped fiber cladding pumping lasers operating at 1.95 µm. However, the conversion efficiency from Tm to Ho emission was relatively low, estimated to be around 40% [7]. In 2022, Beaumont et al. achieved the highest slope efficiency reported to date for a Ho^{3+} doped triple-clad fiber pumped by a Tm^{3+} doped fiber laser at a wavelength exceeding 2.1 µm. Their results showed a slope efficiency of 73% for converting pump light at 1.94 µm to laser light at 2.12 µm, with a maximum output power of 62 W [8]. To simplify the laser system and maintain high efficiency above 2 µm laser wavelength, a Tm^{3+}, Ho^{3+} co-doped fiber can be used as an active medium in the laser source. The study conducted by Ramirez-Martinez et al. on the concentration ratio of Tm^{3+} and Ho^{3+} dopants in co-doped fibers resulted in exceptional conversion efficiencies from 790 nm to 2.10 µm. The study reported a record-breaking 56% conversion efficiency for a Tm^{3+}, Ho^{3+} co-doped single oscillator fiber laser, with a maximum output power of 37 W [9]. In the literature, studies of Tm^{3+}, Ho^{3+} codoped fiber lasers at higher output powers (between 100 W and 300 W) reported lower slope efficiencies, around 45-50% [10,11]. The highest power generated from such fiber laser source was 262 W, reported by Forster et al. in 2022 [10]. The active fiber was pumped in free space and the use of bulk components leads to several limitations in thermal management and robustness of the source that can be reduced in all-fiber architectures. However, using fiber components as in Ref. [11] also introduces new issues, such as power losses and degradation of the output beam profile caused by splices between active and passive fibers with different geometries, as reported by Simakov *et al.* in 2015 [12]. Moreover, the FBG used in a fiber laser

#486723 https://doi.org/10.1364/OE.486723
Journal © 2023 Received 31 Jan 2023; revised 17 Mar 2023; accepted 18 Mar 2023; published 23 May 2023

Optics EXPRESS

cavity can be sensitive to power levels, resulting in spectral degradation due to heating which is characterized by broadening and shifting of the laser output spectrum. This effect was observed in 2016 by Walbaum *et al.* with a monolithic single-oscillator thulium-doped fiber laser source in which the FBG reflected wavelength was shifted from 1966nm at low power to 1970nm at 567 W of output power [13]. Furthermore, the heating of FBGs can result in a phenomenon known as spectral splitting, in which the spectrum is divided into multiple peaks [14,15]. The combination of these three effects (splitting, shifting, broadening) has been recently observed on a 2.09-µm continuous-wave monolithic single-oscillator Tm^{3+}, Ho^{3+} codoped fiber laser source [11]. In this paper, the output spectrum was shifted by 2.4 nm and its spectral bandwidth had doubled between 15 W and 195 W of output power. Nonetheless, the sensitivity of FBGs to temperature changes and mechanical stress is an advantage in some cases. It makes them widely used in stress sensing applications [14–19] and it can be particularly relevant for tunable laser sources [20–22]. However, in high-power laser development activities, these effects act as a performance limitation since they can be responsible for a mismatch between the two FBGs that compose the cavity. For these activities, fortunately recent advancements in FBG fabrication have resulted in a significant reduction of the FBG thermal slope, simplifying the thermal management of the components and reducing both shifting and broadening effects. Additionally, the absorption/emission phenomena occurring in the gain medium can also impact the laser operation. The free-running (without FBG or any wavelength selective element) emission wavelength of a laser depends on the maximum gain of the active fiber, and the length of the fiber is a key parameter that influences on the laser operation. Traditionally, the fiber length is chosen to maximize the pump power conversion efficiency and typically, the cladding-pumped fiber length providing about 13-dB pump absorption is chosen. However, a longer fiber implies a longer wavelength of the maximum gain wavelength and can lead to the presence of a parasitic cavity that can coexist with the main cavity (made with a high-reflectivity FBG) and which depends on this maximum gain wavelength, as mentioned in Ref. [11]. An easy solution to prevent this parasitic oscillation is to cleave the FBG fiber with an angle to avoid Fresnel back reflection at this fiber end facet [23]. In this case, no secondary cavity exists in the cavity and the light transmitted by the HR FBG (around 1% of the power at 2090nm and eventually the light at another wavelength) is lost. An interesting consideration is the potential to optimize the laser performance by aligning the maximum gain wavelength of the fiber with the wavelength imposed by the FBG. Additionally, in certain cases where the maximum gain would allow improving the emission, the use of a 0°-cleaved angle to generate a Fresnel reflection at the end of the FBG fiber may prove being beneficial in reducing losses.

In this study, we investigate the power and spectral evolution of a monolithic all-fiber laser source based on a Tm^{3+}, Ho^{3+}-codoped fiber emitting at 2.1 µm in continuous wave regime. Specifically, we evaluate the impact of matching and mismatching between the maximum fiber gain and the FBG reflected wavelengths on the laser performance and stability. Finally, the 0°- or 8°-cleaved angles of the FBG fiber is analyzed with respect to the matched conditions.

2. Experimental setup

The experimental setup is depicted in Fig. 1. The gain medium is a silica double clad (DC) polarization-maintaining (PM) Thulium-Holmium Doped Fiber (THDF) from *exail* (formerly *iXblue Photonics*) exhibiting a codoped (Tm^{3+} ion concentration: 4 wt.%, Ho^{3+} ion concentration: 0.4 wt.%) core of 20 µm diameter (numerical aperture: NA = 0.11) and a 300-µm circular pump cladding (NA = 0.46). The THDF, cooled by deionized water at 18 °C, is symmetrically pumped by four high-power 793-nm fiber-coupled laser diodes (LD) fusion-spliced to two $(2 + 1) \times 1$ fiber pump combiners (FPC), resulting in a maximum total injected pump power of 472 W (taking into account the 12-% losses induced by the FPCs). The high reflectivity (HR) mirror of the laser cavity is a FBG written in the core of a passive fiber (DC-PM-20-300) reflecting

Optics EXPRESS

intracavity light. The output coupler (OC) consists of the FPC passive fiber cleaved at 0° in order to benefit from the 4-% Fresnel reflection at the air/silica interface. All FBGs utilized in this study were produced by *exail*. They were fabricated in a way to ensure a low thermal coefficient of around 1°C/W, making them less susceptible to temperature increases and thus less likely to cause spectral degradation in fiber laser systems. To actively cool the metal housing of the FBG, we put it in contact with a copper plate cooled by an internal circuit of water maintained at 18°C. All optical fiber components were spliced together using a CO_2 splicer (LZM-100, *Fujikura*). The spectral measurement was performed using a *Yokogawa* Optical Spectrum Analyzer with a wavelength resolution of 0.01 nm. We studied three configurations with different combinations of FBG reflected wavelengths and active fiber lengths, as detailed in Table 1.

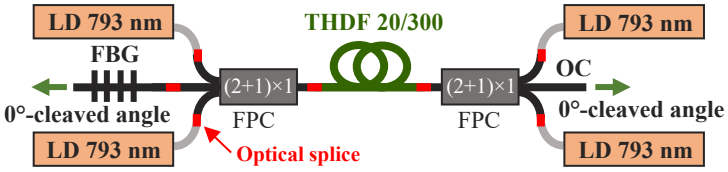

Fig. 1. Experimental setup for the monolithic single-oscillator fiber laser source. Passive and active fibers are represented in black and green lines, respectively. Fiber fusion splices are represented by red marks.

Table 1. Description of the three laser configurations

Configuration	THDF length	FBG wavelength
#1	10 m	2.09 µm
#2	10 m	2.12 µm
#3	5 m	2.09 µm

The reflected optical spectra of the two FBGs used in this study are presented in Fig. 2. The FBG used in configurations #1 and #3 has a reflectivity higher than 98% at 2090.3 nm with a FWHM spectral width of 1.27 nm, as shown in Fig. 2(a). Meanwhile, the FBG used in configuration #2 has a reflectivity higher than 99% at 2120.0 nm and a FWHM spectral width of 1.24 nm, as depicted in Fig. 2(b).

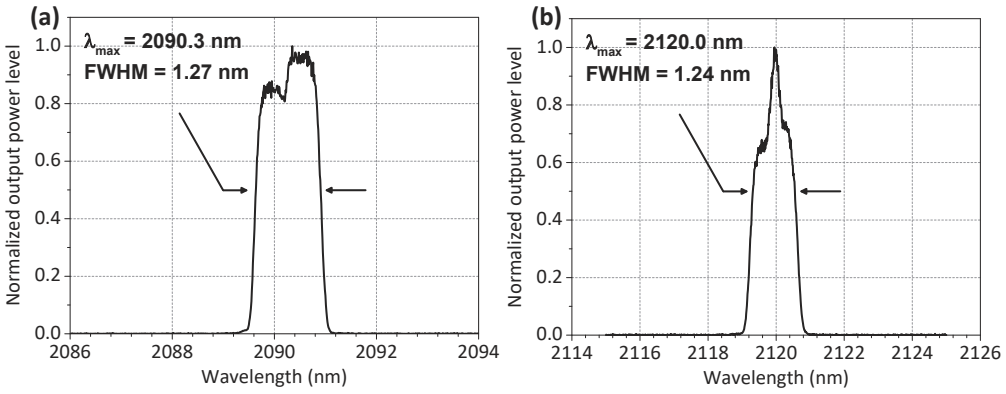

Fig. 2. Optical spectra reflected from 2.09 µm FBG (a) and 2.12 µm FBG (b) in linear scale.

Optics EXPRESS

3. Non-optimized cavity: configuration #1

The 2-µm power measured at the OC and at the FBG outputs (part of light transmitted by the FBG) as a function of the 793-nm pump power injected into the active fiber is shown in Fig. 3(a). At the OC, a maximum power of 146 W was obtained (efficiency: 31%; threshold: 21.2 W). At the FBG side, a maximum 2.1-µm power of 43.4 W was measured. These results demonstrate that a significant portion of the 2.1-µm power generated by the laser is transmitted by the FBG (23%) rather than being reflected to the main output of the source. Additionally, the 2.09-µm power exhibits a slightly non-linear evolution on both sides, which is visible when comparing the measured data to the linear fits as depicted in Fig. 3(a).

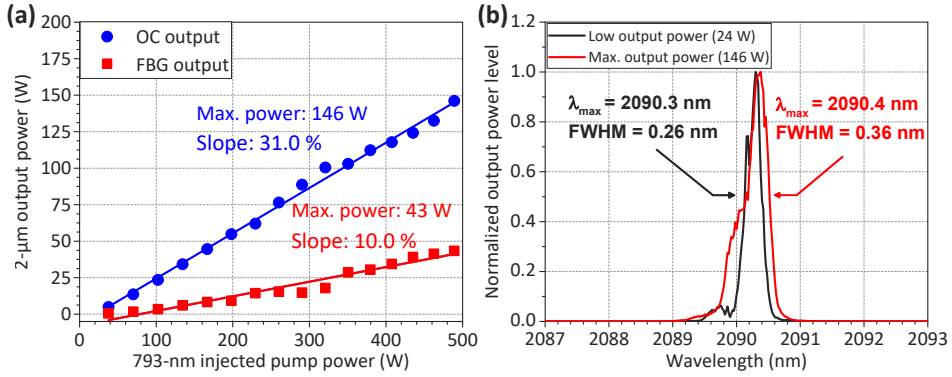

Fig. 3. (a) 2.1-µm power measured at the OC (blue dots) and FBG (red squares) sides versus 793-nm injected pump power; (b) Normalized emission spectrum at the OC at different power levels at 2 µm over a 7 nm spectral band (black: 24 W; red: 146 W).

Spectral measurements (made around 2.09 µm) at the OC at two output power levels are shown in Fig. 3(b), at low power (24 W) and at the maximum output power (146 W). At 24 W, the measured spectrum (FWHM = 0.26 nm) is centered at 2090.3 nm. At 146 W, the spectrum has a center wavelength of 2090.4 nm and a FWHM width of 0.36 nm. The use of a FBG with a low thermal slope greatly reduces the spectral shift and broadening, as evidenced by a 0.1 nm shift and broadening during a power increase from 24 W to 146 W at 2.1 µm. Indeed, in a previous experiment with a similar laser source, but using a standard FBG design with a tenfold higher thermal slope, we observed a significant spectral shift and broadening, with values of 2.4 nm and 0.6 nm, respectively [11]. Moreover, using the low thermal FBG resulted in less splitting into multipeaks around the central line at high power. These results confirm that heating of the FBG when increasing the power is a major contributor to these phenomena, as previously established in Refs. [14–19]. Figure 4 illustrates the emission spectrum on the OC side (Fig. 4(a)) and on the FBG side (Fig. 4(b)) at the maximum output power across a broad measurement range, shown in logarithmic scales. The measurement at the OC reveals the presence of secondary peaks at around 2.12 µm, with a peak power level of -9.0 dB relative to the primary peak (as seen in Fig. 4(b)). Based on analysis of these spectra, it is estimated that at the maximum output power, 34.3% of the signal power at the OC originates from the secondary peaks. The spectral analysis of the FBG transmitted radiation reveals that the dominant proportion of the signal light is emitted at a wavelength around 2.12 µm. Indeed, at maximum output power, the secondary peaks around 2.12 µm have a peak power level of +8.9 dB relative to the spectral component at 2090nm (as seen in Fig. 4(b)).

Figure 5 depicts the proportion of signal power at 2.12 µm (secondary peaks) at the output of the OC and at the output of the FBG as a function of the 793-nm injected pump power. The data shows that the proportion of power at 2.12 µm increases with increasing power. The OC

Optics EXPRESS

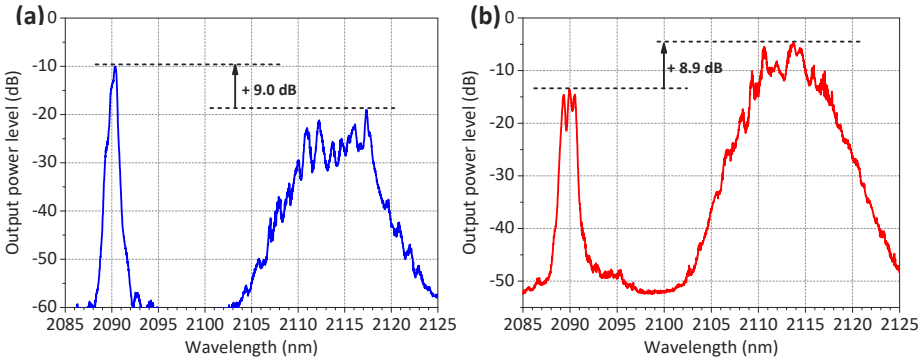

Fig. 4. Emission spectrum of the 2.1-µm fiber laser on the OC side (a) and on the FBG side (b), at the maximum output power, measured with a broad spectral band of 40 nm illustrating secondary peaks around 2120 nm.

output shows a chaotic evolution, plateauing at around 40% at 400 W of pump power and above, while the proportion of power at the FBG output increases sharply to more than 90% for pump powers exceeding 150 W. The higher proportion of power at 2.12 µm in FBG transmission is not surprising, as its reflectivity band is centered at 2.09 µm, which acts as a filter by reflecting most of the light at 2.09 µm and transmitting the signal at 2.12 µm.

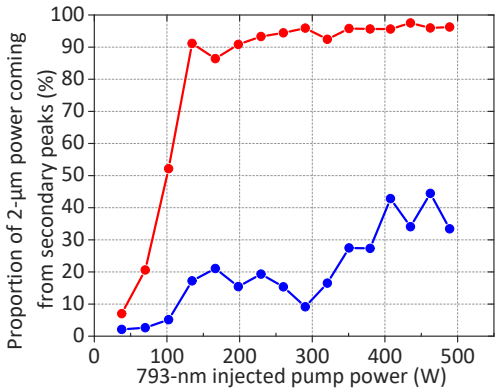

Fig. 5. Proportion of power from secondary peaks around 2.12 µm at the output of the OC (blue dots) and at the output of the FBG (red dots) as a function of the pump power injected at 793 nm.

As demonstrated in Ref. [11], by the use of a Fresnel cavity configuration (free-running cavity without FBG to impose the emitted wavelength), these secondary peaks observed around 2.12 µm are the result of the natural emission of the laser source, corresponding to the highest absorption gain of the 10-m long piece of active fiber. As the maximum gain wavelength depends on the fiber length, it suggests that a different length of active fiber can result in the formation of a parasitic cavity at a different wavelength. This secondary cavity may be suppressed with an 8°-cleaved angle of the FBG fiber to avoid Fresnel back-reflection [23]. However, in the following study, we investigate potential laser efficiency enhancement generated by utilizing a FBG at 2.12 µm instead of 2.09 µm in conjunction with a 10-m long piece of active fiber (configuration #2). Additionally, we explore the use of an optimal fiber length to achieve the highest absorption gain at 2.09 µm with the corresponding FBG (configuration #3). The presence of the Fresnel back

Optics EXPRESS

reflections by maintaining a 0°-cleaved angle will be evaluated in these two configurations in which the maximum gain wavelength matches the FBG parameters.

4. Study on the adaptation of FBG reflectivity to fiber gain

4.1. Adaptation of the FBG reflection to the gain of the 10-m fiber: configuration #2

In this configuration, the 2.12-µm FBG presented in Fig. 2(b), has been integrated into the laser source to match the FBG reflection wavelength to the maximum gain wavelength of the 10-m active fiber. Figure 6(a) illustrates the power measurements at 2.1 µm at the output of the OC and at the output of the FBG at 2.12 µm, as a function of the injected 793-nm pump power. The maximum power of 153.6 W at 2.1 µm was obtained at the output of the OC, yielding a slope efficiency of 33.7% and a lasing threshold of 29.9 W. At the FBG fiber output, a maximum power of 12.2 W at 2.1 µm was recorded. This matched configuration resulted in a 6.6 W increase in output power and a + 2.7 percentage points increase in slope efficiency, as well as an almost linear power evolution. Moreover, it is worth noting that the proportion of power transmitted by the FBG (7.3%) is lower than the 23% measured in the mismatched configuration #1.

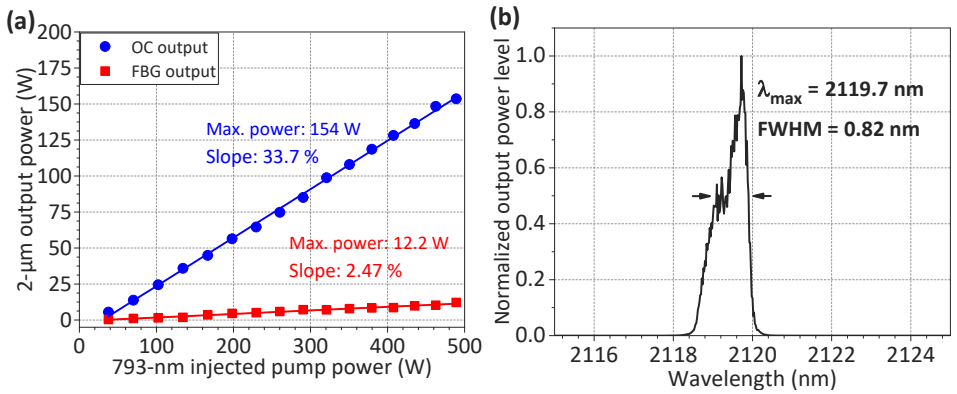

Fig. 6. (a) 2.1-µm laser power measured at the OC output (blue dots), FBG output (red squares) versus 793-nm injected pump power in configuration #2; (b) Emission spectrum at the OC using a 2.12 µm FBG with a cleaved fiber end angle of 0°.

The spectral measurement at the OC output is shown in Fig. 6(b). The spectrum has a FWHM width of 0.82 nm and a center wavelength of 2119.8 nm at maximum output power. These results indicate that there is no disturbance from a parasitic cavity when the reflectivity of the FBG is matched to the gain of the active fiber. According the wavelength reflectivity of the FBG with the maximum gain of the 10-m fiber slightly improved the OC output power and efficiency. The limited improvement observed in this laser configuration can be mostly attributed to the quality of splicing. Unlike configurations #1 and #3, the intra-cavity splicing between the active fiber and the passive fibers of the combiners has not been optimized in this configuration due to equipment failure. In contrast, configurations #1 and #3 utilized optimized splicing parameters determined through an active splicing method outlined in Ref. [11], including heating time and heating power. Splices with optimized parameters exhibit minimal losses, near to 1% at 2.1 µm. In configuration #2, the random nature of the splices makes it challenging to predict the losses accurately. However, since measurements in Fresnel cavity configuration (cavity made by two 0°-cleaved angle fiber providing 4-% Fresnel reflection) demonstrated a maximal output power of 198 W, we might suppose that almost 15% of power is lost.

In order to measure the impact of the presence of the secondary cavity formed by the 0°-cleaved angle of the FBG fiber on the laser performances, the same measurements were conducted

Optics EXPRESS

with now a cleave of the fiber at 8°. The fiber length was still 10 m and the cavity was still closed by the 2.12-µm FBG. As seen in Fig. 7(a), the maximum output power was 154.7 W, corresponding to an optical efficiency of 34.7%. So, both the efficiency and the output power are slightly increased and, moreover, the power evolution is perfectly linear when not perturbed by the parasitic oscillation, even if it happens at the same wavelength. As shown in Fig. 7(b), the spectrum obtained at maximum power with an 8° cleave angle is comparable to the results obtained with a 0° cleave angle, with a central wavelength of 2119.8 nm and a FWHM width of 0.72 nm. Moreover, the comparison of the results with a 0°- and an 8°-cleaved angle, respectively, shows that the system is globally more stable when the secondary cavity is suppressed.

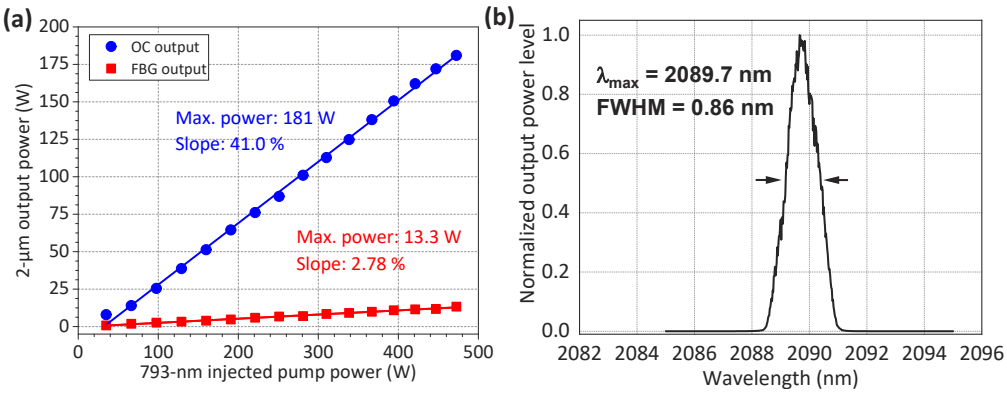

Fig. 7. (a) 2.1-µm laser power measured at the OC output (blue dots), FBG output (red squares) versus 793-nm injected pump power in configuration #2; (b) Emission spectrum at the OC using a 2.12 µm FBG with a cleaved fiber end angle of 8°.

4.2. Adaptation of the active fiber length to the 2.09 µm FBG: configuration #3

In the third experiment, the wavelength with the highest gain in the fiber was matched to the reflectivity wavelength of the FBG at 2.09 µm (Fig. 2(a)). This was done by shortening the length of the fiber to 5 m, a value which was derived from previous experimental works [24], which also used the same active fiber. The goal was to match the maximum gain at 2.09 µm. In contrast to configuration #2 using a 2.12 µm FBG, the 2.09 µm FBG was integrated with a source that featured optimized splices. Figure 8(a) shows the measurements of laser power at 2.1 µm at the output of the OC and at the output of the FBG, as a function of the pump power at 793 nm injected into the 5-m long active fiber. A maximum laser power of 179 W at 2.1 µm was achieved at the OC output, resulting in a slope efficiency of 40.2% and a lasing threshold of 39.2 W (Fig. 8(a)). The output of the FBG fiber reached a maximum power of 12.9 W at 2.1 µm. The proportion of the total output power transmitted by the FBG is significantly lower in comparison to the unmatched configuration #1 (6.7% versus 23%). Moreover, we can note an important increase in OC output power and efficiency, with +33.1 W and +9.2 percentage points, respectively, compared to the configuration #1.

The spectral measurements of the OC output in the given configuration, displayed in Fig. 8(b), revealed a spectrum with a center wavelength of 2090.0 nm and a FWHM of 0.80 nm at the maximum output power. In comparison, in configuration #1, using the same 2.09 µm FBG with a 10-m active fiber length (Fig. 3(b)), the laser exhibited a spectral width of 0.4 nm, which is half the width of the current configuration. It suggests that the difference in spectral width is likely due to the broadness of the natural emission of the laser rather than to the FBGs.

With a fiber length of 5 m and an absorption of 3.5 dB/m, a significant portion of the pump power is still absorbed, resulting in 16 W of residual pump at the output (8 W when using a 10-m

Optics EXPRESS

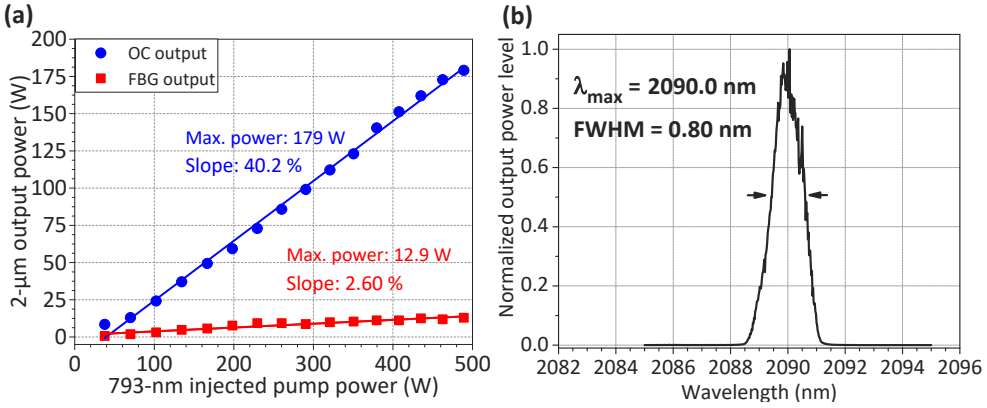

Fig. 8. (a) 2.1-µm power measured at the OC output (blue dots) and the FBG output (red dots) versus 793-nm injected pump power in configuration #3; (b) Emission spectrum at the OC using a 2.09 µm FBG with a cleaved fiber end angle of 0°.

length of fiber). Although slightly less pump power was absorbed with a 5-m fiber compared to a 10-m fiber, the 2.09-µm matching (configuration #3) was found to be more efficient than the 2.12-µm matching (configuration #2) likely due to a combination of factors including higher silica absorption and Stokes efficiency at the 2.12-µm wavelength and less optimized splices in this version of laser.

In line with configuration #2, an experiment was performed with an 8° angle cleave at the end of the 2.09 µm FBG fiber. The results of power and spectrum measurements are depicted in Fig. 9. A maximum output power of 181.0 W at 2.1 µm was achieved at the OC, with a slope efficiency of 41.0% (Fig. 9(a)). At the FBG output, the maximum obtained power was 13.3 W. The results of power and slope efficiency showed a slight improvement with an 8° cleave angle compared to a 0° cleave angle, as observed in the study on the FBG at 2.12 µm in configuration #2. The spectrum at maximum power, shown in Fig. 9(b), had a central wavelength of 2089.7 nm and an FWHM width of 0.86 nm, similar to the findings in Fig. 8(b). The results indicate that the 8° cleave angle at the FBG fiber end had no significant impact on the spectral behavior of the laser in a configuration where the FBG reflectivity and fiber gain are in agreement.

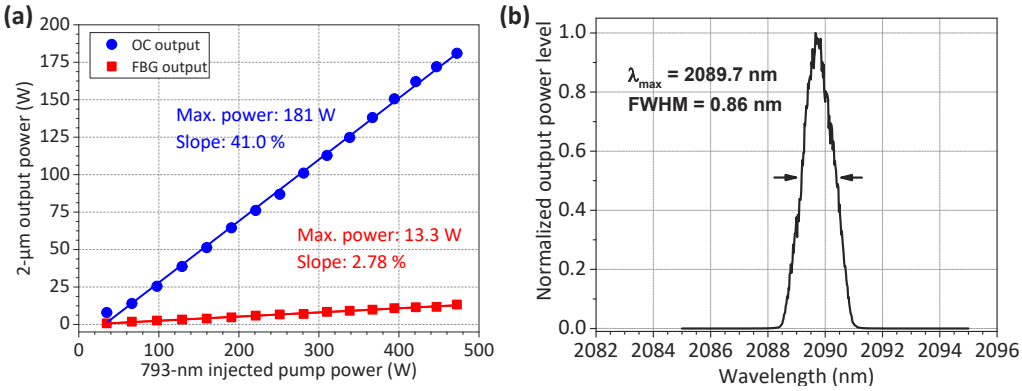

Fig. 9. (a) 2.1-µm power measured at the OC output (blue dots) and the FBG output (red dots) versus 793-nm injected pump power in configuration #3; (b) Emission spectrum at the OC using a 2.09 µm FBG with a cleaved fiber end angle of 8°.

Optics EXPRESS

5. Conclusion

This study investigated the power and spectral properties of an all-fiber laser source based on a Tm^{3+}, Ho^{3+}-codoped fiber emitting at 2.1 µm in continuous wave mode of operation. In monolithic fiber lasers, a parasitic cavity can be formed between the two end facets that are cleaved at a 0° angle (4-% reflectivity). This parasitic cavity coexists with the main cavity created by the high-reflectivity mirror and the output coupler. The parasitic cavity can lead to a secondary emission at a wavelength imposed by the maximum gain wavelength, which depends on the length of the active fiber. When the maximum gain wavelength does not match the emission wavelength imposed by the FBG, the parasitic emission causes a loss of efficiency at the desired wavelength, resulting in a mismatched cavity. In this study, we presented a first mismatched configuration where a large proportion, more than 34%, of the OC output power was generated at a parasitic wavelength of 2.12 µm and 23% of the total power was transmitted through the 2.09-µm FBG. We analyzed the effect of matching the maximum fiber gain with the FBG reflected wavelength on the laser performance. In order to match the two parameters using the same 10-meter piece of active fiber as for the first configuration, we replaced the 2.09-µm FBG with one centered at 2.12 µm. This new configuration resulted in a reduction of power loss on the FBG side to 8% while ensuring that all the power was emitted at the desired 2.12-µm wavelength. In a final configuration, we reduced the active fiber length to 5 m to match the peak fiber gain with the 2.09-µm FBG. This resulted in a significant improvement in performance, specifically a 33 W increase in output power at 2.09 µm, as well as an improvement of +9.2 percentage points in slope efficiency, reaching a maximum output power of 179 W at the OC and a slope efficiency of as high as 40.2%. The overlapping wavelengths between the main and the secondary cavities prevent the formation of secondary spectral peaks. However, when matching the two emissions, the spectral width of the main peak seems to be broadened (0.80 nm of FWHM) as compared to the mismatched cavity (0.36 nm). Moreover, our experiments involving an 8° cleave of the FBG fiber end in order to eliminate the parasitic cavity revealed a modest improvement in laser output power, slope efficiency, and linearity of power evolution for both matched configurations. These results indicate that even when the reflectivity of the FBG and the maximum gain of the fiber are matched, the parasitic cavity still exerts a minor influence on the laser performance.

Funding. Bundesamt für Ausrüstung, Informationstechnik und Nutzung der Bundeswehr; Direction Générale de l'Armement.

Acknowledgments. Portions of this work were presented at the Advanced Solid-State Lasers Conference in 2022, FBG reflected wavelength and fiber gain matching on a continuous wave monolithic Tm^{3+}, Ho^{3+}-doped fiber laser.

Disclosures. The authors declare no conflicts of interest.

Data availability. Data underlying the results presented in this paper are not publicly available at this time but may be obtained from the authors upon reasonable request.

References

1. S. Jackson, A. Sabella, and D. Lancaster, "Application and development of high-power and highly efficient silica-based fiber lasers operating at 2 µm," IEEE J. Select. Topics Quantum Electron. **13**(3), 567–572 (2007).
2. J. Cariou, B. Augere, and M. Valla, "Laser source requirements for coherent lidars based on fiber technology," C. R. Phys. **7**(2), 213–223 (2006).
3. A. Hemming, N. Simakov, J. Haub, and A. Carter, "A review of recent progress in holmium-doped silica fibre sources," Opt. Fiber Technol. **20**(6), 621–630 (2014).
4. M. C. Pierce, S. D. Jackson, M. R. Dickinson, and T. A. King, "Laser-tissue interaction with a high-power 2-microm fiber laser: preliminary studies with soft tissue," Lasers Surg. Med. **25**(5), 407–413 (1999).
5. D. Pal, A. Ghosh, R. Sen, and A. Pal, "Continuous-wave and quasi continuous-wave thulium-doped all fiber laser: implementation on kidney stone fragmentations," Appl. Opt. **55**(23), 6151–6155 (2016).
6. L. Shah, R. A. Sims, P. Kadwani, C. C. Willis, J. B. Bradford, A. Sincore, and M. Richardson, "High-power spectral beam combining of linearly polarized Tm:fiber lasers," Appl. Opt. **54**(4), 757–762 (2015).
7. A. Hemming, N. Simakov, A. Davidson, S. Bennetts, M. Hughes, N. Carmody, P. Davies, L. Corena, D. Stepanov, J. Haub, R. Swain, and A. Carter, "A monolithic cladding pumped holmium-doped fibre laser," in *CLEO: 2013, OSA Technical Digest (online)* (Optica Publishing Group, 2013), paper CW1M.1.

Optics EXPRESS

8. B. Beaumont, P. Bourdon, A. Barnini, L. Kervella, T. Robin, and J. Le Gouët, "High Efficiency Holmium-Doped Triple-Clad Fiber Laser at 2120 nm," J. Lightwave Technol. **40**(19), 1–6 (2022).
9. N. J. Ramírez-Martínez, M. Núñez-Velázquez, and J. K. Sahu, "Study on the dopant concentration ratio in thulium-holmium doped silica fibers for lasing at 2.1 µm," Opt. Express **28**(17), 24961–24967 (2020).
10. P. Forster, C. Romano, J. Schneider, M. Eichhorn, and C. Kieleck, "High-power continuous-wave Tm^{3+}:Ho^{3+}-codoped fiber laser operation from 2.1 µm to 2.2 µm," Opt. Lett. **47**(10), 2542–2545 (2022).
11. A. Motard, C. Louot, T. Robin, B. Cadier, I. Manek-Hönninger, N. Dalloz, and A. Hildenbrand-Dhollande, "Diffraction limited 195-W continuous wave laser emission at 2.09 µm from a Tm^{3+}, Ho^{3+}-codoped single-oscillator monolithic fiber laser," Opt. Express **29**(5), 6599–6607 (2021).
12. N. Simakov, A. V. Hemming, A. Carter, K. Farley, A. Davidson, N. Carmody, M. Hughes, J. M. O. Daniel, L. Corena, D. Stepanov, and J. Haub, "Design and experimental demonstration of a large pedestal thulium-doped fibre," Opt. Express **23**(3), 3126–3133 (2015).
13. T. Walbaum, M. Heinzig, T. Schreiber, R. Eberhardt, and A. Tünnermann, "Monolithic thulium fiber laser with 567Woutput power at 1970nm," Opt. Lett. **41**(11), 2632–2635 (2016).
14. G. Rajan, M. Ramakrishnan, Y. Semenova, E. Ambikairajah, G. Farrell, and G.-D. Peng, "Experimental Study and Analysis of a Polymer Fiber Bragg Grating Embedded in a Composite Material," J. Lightwave Technol. **32**(9), 1726–1733 (2014).
15. X. Zhang, J.-J. Max, X. Jiang, L. Yu, and H. Kassi, "Experimental investigation on optical spectral deformation of embedded FBG sensors," Proc. SPIE **6478**, 647808 (2007).
16. G. Meltz, W. W. Morey, and W. H. Glenn, "Formation of Bragg gratings in optical fibers by a transverse holographic method," Opt. Lett. **14**(15), 823–825 (1989).
17. A. Rajabzadeh, R. Heusdens, R. Hendriks, and R. Groves, "Calculation of the mean strain of smooth non-uniform strain fields using conventional FBG sensors," J. Lightwave Technol. **36**(17), 3716–3725 (2018).
18. V. Mishra, M. Lohar, and A. Amphawan, "Improvement in temperature sensitivity of FBG by coating of different materials," Optik **127**(2), 825–828 (2016).
19. K. Peters, P. Pattis, J. Botsis, and P. Giaccari, "Experimental verification of response of embedded optical fiber Bragg grating sensors in non-homogeneous strain fields," Opt. Lasers Eng. **33**(2), 107–119 (2000).
20. J. M. O. Daniel, N. Simakov, M. Tokurakawa, M. Ibsen, and W. A. Clarkson, "Ultra-short wavelength operation of a thulium fibre laser in the 1660–1750nm wavelength band," Opt. Express **23**(14), 18269–18276 (2015).
21. C. S. Goh, S. Y. Set, and K. Kikuchi, "Widely tunable optical filters based on fiber Bragg gratings," IEEE Photon. Technol. Lett. **14**(9), 1306–1308 (2002).
22. P. S. André, J. L. Pinto, I. Abe, H. J. Kalinowski, O. Frazão, and F. M. Araújo, "Fibre Bragg Grating for Telecommunications Applications: Tuneable Thermally Stress Enhanced OADM," J. Microw. Optoelectron. Electromagn. **2**(3), 32–45 (2001).
23. C. Louot, A. Motard, T. Ibach, I. Manek-Hönninger, T. Robin, B. Cadier, N. Dalloz, and A. Hildenbrand-Dhollande, "High-efficiency 2.09 µm single-oscillator monolithic thulium-doped fiber laser," IEEE Photon. Technol. Lett. (to be published).
24. N. Dalloz, T. Robin, B. Cadier, C. Kieleck, M. Eichhorn, and A. Hildenbrand-Dhollande, "55 W actively Q-switched single oscillator Tm^{3+}, Ho^{3+}-codoped silica polarization maintaining 2.09 µm fiber laser," Opt. Express **27**(6), 8387–8394 (2019).